

Control Stratification in Drying Particle Suspensions via Temperature Gradients

Yanfei Tang (唐雁飞),¹ Gary S. Grest,² and Shengfeng Cheng (程胜峰)¹

¹*Department of Physics, Center for Soft Matter and Biological Physics, and Macromolecules Innovation Institute, Virginia Polytechnic Institute and State University, Blacksburg, Virginia 24061, USA*

²*Sandia National Laboratories, Albuquerque, NM 87185, USA*

(Dated: April 26, 2022)

A potential strategy for controlling stratification in a drying suspension of bidisperse particles is studied using molecular dynamics simulations. When the suspension is maintained at a constant temperature during fast drying, it can exhibit “small-on-top” stratification with an accumulation (depletion) of smaller (larger) particles in the top region of the drying film, consistent with the prediction of current theories based on diffusiophoresis. However, when only the region near the substrate is thermalized at a constant temperature, a negative temperature gradient develops in the suspension because of evaporative cooling at the liquid-vapor interface. Since the associated thermophoresis is stronger for larger nanoparticles, a higher fraction of larger nanoparticles migrate into the interfacial region of the drying film at fast evaporation rates. As a result, stratification is converted to “large-on-top”. Very strong “small-on-top” stratification can be produced with a positive thermal gradient in the drying suspension. Here we explore a way to produce a positive thermal gradient by thermalizing the vapor at a temperature higher than that of the solvent. Possible experimental approaches to realize various thermal gradients in a suspension undergoing solvent evaporation, and thus different stratifying states in the drying film, are suggested.

I. INTRODUCTION

The drying of colloidal suspensions has been studied for several decades.[1–17] Recently, drying-induced stratifying phenomena in polydisperse colloidal mixtures have attracted great attention,[6, 7, 18–33] as they point to a quick, facile, one-pot method of depositing layered multifunctional coating films on a surface. In a particle suspension undergoing drying, the vertical distribution of particles is controlled by the Péclet number, $Pe = Hv_e/D$, where H a characteristic length scale in the problem and can be taken as the film thickness, v_e is the receding speed of the liquid-vapor interface during evaporation, and D is the diffusion coefficient of the particle.[9, 34] The Péclet number characterizes the competition between diffusion and evaporation-induced particle migration. When $Pe \gg 1$, particles build up near the interface and their final distribution in the dry film may develop gradients; while for $Pe \ll 1$, the particles diffuse fast enough to mitigate evaporative effects and are expected to be uniformly distributed in the deposited film.[9] When particles are large, gravity cannot be ignored and sedimentation can come into play.[7, 29]

In the case of a suspension of a bidisperse mixture of particles made from the same material but having different diameters, d_l and d_s , the final distribution of particles is determined by two Péclet numbers, Pe_l and Pe_s , for the large and small particles, respectively. If the Stokes-Einstein relationship holds, then $Pe_l/Pe_s = d_l/d_s > 1$. When $Pe_l > 1 > Pe_s$, Trueman *et al.* found the so-called “large-on-top” stratification,[12, 13] where the larger (smaller) particles are enriched (depleted) near the receding interface. Recently, Fortini *et al.* discovered counterintuitive “small-on-top” stratification in the regime of $Pe_l > Pe_s \gg 1$, i.e., when the drying is extremely rapid.[18, 21] Since then, a number of experimental,[19,

24, 27, 29, 31, 33] theoretical,[20, 25, 26] and simulation [22, 23, 28, 30, 32] studies have been reported on the stratifying phenomena in drying suspensions of polydisperse particles and their physical mechanisms. The idea of diffusiophoresis being responsible for “small-on-top” stratification is widely supported.[18, 20, 22, 25, 26, 30] In this picture, when $Pe_s \gg 1$ and the volume fraction of the smaller particles, ϕ_s , is above certain threshold that depends on Pe_s , the smaller particles congregate near the receding interface during evaporation and their distribution develops a gradient that decays into the drying film. This gradient tends to push the larger particles out of the interfacial region and consequently the larger particles are depleted near the interface, resulting in “small-on-top” stratification.

The key ingredient of the diffusiophoretic model is that the cross-interaction between the large and small particles has asymmetric effects on the phoretic drift of particles and drives the larger ones away from the interfacial region faster than the smaller ones.[20, 25] Therefore, the size asymmetry, quantified as $\alpha = d_l/d_s$, is a crucial parameter that controls the outcome of stratification, with larger α favoring “small-on-top” stratification. Martín-Fabiani *et al.* studied a system with the smaller particles coated with hydrophilic shells and explored the effect of changing the pH of the initial dispersion.[19] In a dispersion with low pH, α is large enough to lead to “small-on-top” stratification. When the pH is raised, α is reduced as the hydrophilic shells swell substantially, and stratification is switched off.

The approach of Martín-Fabiani *et al.* can be used for systems where the particle size can be tuned with external stimuli.[19] However, other possible approaches of controlling stratification for systems with fixed particle sizes have rarely been explored. In a previous work,[30] we used molecular dynamics (MD) modeling to study

drying suspensions of a binary mixture of nanoparticles and found that for fast evaporation rates, the solvent can develop a negative temperature gradient toward the interface because of evaporative cooling effect. This temperature gradient induces thermophoresis, in which the larger particles are pushed more strongly into the interfacial region where the temperature is lower and the solvent density is higher. The competition between thermophoresis generated by evaporative cooling and diffusiophoresis can thus suppress “small-on-top” stratification at ultra fast drying rates or even turn the stratification into “large-on-top”. This discovery further indicates that thermophoresis, with a controlled thermal gradient other than the naturally occurring evaporative cooling, may be used to control stratification. In this paper, we employ MD modeling to test this idea in detail and demonstrate that stratification in a drying suspension can be controlled on demand with a temperature gradient imposed on the system, i.e., via controlled thermophoresis.

II. METHODS

We performed MD simulations on a suspension of a bidisperse mixture of nanoparticles.[30] The solvent is modeled explicitly as beads of mass m and interacting with each other via a Lennard-Jones (LJ) potential, $U_{\text{LJ}}(r) = 4\epsilon [(\sigma/r)^{12} - (\sigma/r)^6 - (\sigma/r_c)^{12} + (\sigma/r_c)^6]$, where r is the center-to-center distance between beads, ϵ is an energy scale, σ is a length scale, and the potential is truncated at $r_c = 3\sigma$. The nanoparticles are modeled as spheres with a uniform distribution of LJ beads at a mass density $1.0m/\sigma$. [35, 36] The large nanoparticles (LNPs) have diameter $d_l = 20\sigma$ and mass $m_l = 4188.8m$, while the small nanoparticles (SNPs) have diameter $d_s = 5\sigma$ and mass $m_s = 65.4m$. The size ratio is $\alpha = 4$. The nanoparticle-nanoparticle interactions are given by integrated forms of a LJ potential for spheres with a Hamaker constant, A_{nn} , characterizing the interaction strength.[35, 36] In this study, $A_{\text{nn}} = 39.48\epsilon$. To ensure that nanoparticles are well dispersed in the initial suspension, the nanoparticle-nanoparticle interactions are rendered purely repulsive by truncating them at 20.574σ , 13.085σ , and 5.595σ for the LNP-LNP, LNP-SNP, and SNP-SNP pairs, respectively. The nanoparticle-solvent interactions are described by similar integrated forms of a LJ potential with a Hamaker constant $A_{\text{ns}} = 100\epsilon$ and a cutoff length $d/2 + 4\sigma$, where d is the nanoparticle diameter.[37]

The entire system consists of $\sim 7 \times 10^6$ LJ beads, 200 LNPs, and 6400 SNPs. The system is placed in a rectangular simulation cell of dimensions $L_x \times L_y \times L_z$, where $L_x = L_y = 201\sigma$, and $L_z = 477\sigma$. The liquid-vapor interface is in the x - y plane, in which periodic boundary conditions are imposed. In the initial suspension, the thickness of the liquid film is about 304σ . The volume fractions of LNPs and SNPs in the initial dispersion are

$\phi_l = 0.068$ and $\phi_s = 0.034$, respectively. Along the z -axis, all the particles are confined in the simulation cell by two walls at $z = 0$ and $z = L_z$. The particle-wall interaction is given by a LJ-like 9-3 potential, $U_W(h) = \epsilon_W [(2/15)(D_W/h)^9 - (D_W/h)^3 - (2/15)(D_W/h_c)^9 + (D_W/h_c)^3]$, where the interaction strength $\epsilon_W = 2.0\epsilon$, h is the distance between the particle center and the wall, and h_c is the cutoff length of the potential. For the solvent beads, $D_W = 1\sigma$ and $h_c = 3\sigma$ (0.8583σ) at the lower (upper) wall. With these parameters, the liquid solvent completely wets the lower wall while the upper wall is purely repulsive. For the nanoparticles, both walls are repulsive with $D_W = d/2$ and $h_c = 0.8583D_W$, where d is the nanoparticle diameter.

To model evaporation of the solvent, a rectangular box of dimensions $L_x \times L_y \times 20\sigma$ at the top of the simulation cell was designated as a deletion zone and a certain number (ζ) of vapor beads of the solvent in this zone were removed every τ , where τ is the reduced unit of time. In this paper, two evaporation rates $\zeta = 30$ and $\zeta = 5$ are adopted. At these rates, the liquid-vapor interface retreats during evaporation at almost a constant speed, v_e . The value of v_e is determined for each evaporating suspension by directly computing the location of the interface as a function of time. The diffusion coefficients of nanoparticles are calculated with direct, independent simulations and the results are $D_l = 1.76 \times 10^{-3}\sigma^2/\tau$ for LNPs and $D_s = 1.55 \times 10^{-2}\sigma^2/\tau$ for SNPs at the initial volume fractions of nanoparticles prior to evaporation (see the Supporting Information). The ratio $D_s/D_l = 8.8$ is higher than $\alpha = 4$, the value expected from the Stokes-Einstein relation because of the finite concentrations of nanoparticles.[38] With values of D_l , D_s , v_e , and H determined, the Péclet numbers for LNPs and SNPs, Pe_l and Pe_s , are computed for each evaporating system.

The Large-scale Atomic/Molecular Massively Parallel Simulator (LAMMPS)[39] was employed for all the simulations reported here. A velocity-Verlet algorithm with a time step $\delta t = 0.01\tau$ was used to integrate the equation of motion, where $\tau = \sigma(m/\epsilon)^{1/2}$ is the LJ unit of time. In the thermalized zone(s) specified for each system, a Langevin thermostat with a small damping rate $\Gamma = 0.01\tau^{-1}$ was used for the solvent beads.

III. RESULTS AND DISCUSSION

Our goal is to demonstrate that a temperature gradient and the associated thermophoretic effect can be used to control stratification in a drying suspension of a polydisperse mixture of nanoparticles. We have previously shown that particles of different sizes have different thermophoretic responses to a thermal gradient.[30] In our previous work, only a thin layer of the liquid solvent adjacent to the bottom wall is thermalized at T_l during evaporation, as shown in Fig. 1(a). Because of evaporative cooling at the liquid-vapor interface, a negative temperature gradient develops and its magnitude is larger for

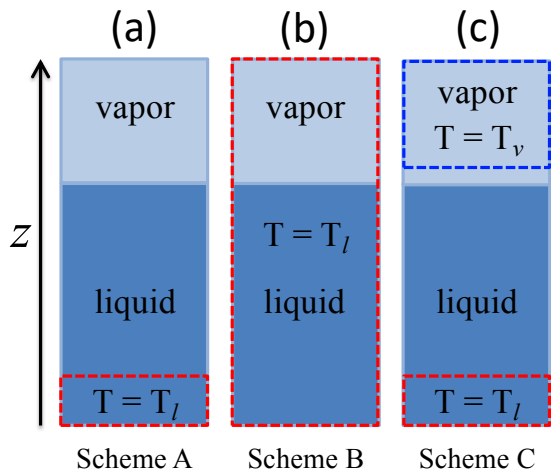


FIG. 1. Schematics of three types of thermalizations during solvent evaporation: (a) Only a thin layer of the liquid solvent adjacent to the bottom wall is thermalized at T_l ; (b) All the liquid and vapor are thermalized at T_l ; (c) A thin layer of the liquid solvent adjacent to the bottom wall is thermalized at T_l while the vapor zone at some distance away from the equilibrium liquid-vapor interface is thermalized at T_v . We set $T_l = 1.0\epsilon/k_B$ while T_v can be higher or lower than T_l to create a thermal gradient.

faster evaporation rates. The negative thermal gradient induces a positive gradient of the solvent density toward the interface, which generates a driving force to transport nanoparticles into the interfacial region.[40, 41] The thermophoretic driving force is stronger for larger particles. For $A_{ns} = 100\epsilon$, SNPs show very weak or even no thermophoretic response (see the Supporting Information). As a result, for very fast evaporation more LNPs than SNPs are driven toward the interface in a drying bidisperse suspension.[30] The thermophoresis caused by evaporative cooling competes with the diffusiophoresis that leads to “small-on-top” stratification at fast drying rates, which is why only weak “small-on-top” stratification was observed in our previous simulations.[30] In certain cases the “small-on-top” stratification expected by the existing theory [25] was even converted to “large-on-top” in the presence of strong thermophoresis.[30]

Based on the physical picture depicted above, it is natural to investigate the effects of a controlled thermal gradient on stratification in a drying suspension. In this paper, we explore this idea by comparing three types of thermalization schemes as sketched in Fig. 1. The Scheme A is the same as in our previous work in which only a 10σ thick layer of the liquid solvent at the bottom of the suspension is thermalized at T_l [Fig. 1(a)]. Evaporative cooling leads to a negative temperature gradient in the suspension toward the interface. In Scheme B, all the solvent beads in the simulation cell are thermalized at T_l [Fig. 1(b)] and thus there are no thermal gradients during evaporation. In Scheme C, in addition to a liquid layer of thickness 10σ thermalized at T_l near the bottom wall, the vapor beads with z -coordinates between $L_z - 150\sigma$

and L_z are thermalized at T_v [Fig. 1(c)]. In this way, a positive (negative) thermal gradient is imposed if $T_v > T_l$ (if $T_v < T_l$), and the magnitude of the gradient is controlled by $|T_v - T_l|$ and the thickness of the film. For all the systems studied in this paper, $T_l = 1.0\epsilon/k_B$. For Scheme C, T_v is varied from $0.75\epsilon/k_B$ to $1.2\epsilon/k_B$.

For Scheme A, the systems are labeled as $T_{1.0}^l\zeta_y$ where the subscript y denotes the value of ζ . For Scheme B, $T_{1.0}\zeta_y$ is used to emphasize that the entire system is maintained at $1.0\epsilon/k_B$ during evaporation. For Scheme C, the systems are labeled as $T_{1.0}^lT_x\zeta_y$, where x indicates the value of T_v . All the systems studied are listed in Table I. $T_{1.0}^lT_{1.1}^v\zeta_5$ and $T_{1.0}^lT_{1.05}^v\zeta_5$ have results in line with $T_{1.0}^lT_{1.2}^v\zeta_5$. We also studied systems with $\zeta = 5$ and $T_v < T_l$, which show negative thermal gradients in the suspension and thermophoresis similar to those in $T_{1.0}^l\zeta_{30}$ and $T_{1.0}^l\zeta_5$ where evaporative cooling occurs. However, we observed condensation of droplets in the vapor phase if T_v is made lower than the temperature at the liquid-vapor interface in Scheme A with the same ζ . Despite this unwanted effect, cooling the vapor at a temperature lower than that of the suspension could be one experimental approach to apply a negative thermal gradient for systems which evaporate slowly or for which the effect of evaporative cooling is not as strong as that of the model LJ liquid employed in our simulations. The last five systems in Table I with T_v varying from $0.75\epsilon/k_B$ to $1.1\epsilon/k_B$ are included in the Supporting Information. In the main text we focus on the first five systems in Table I.

Snapshots of the first five nanoparticle suspensions in Table I during solvent evaporation are shown in Fig. 2. For $T_{1.0}^l\zeta_{30}$ and $T_{1.0}^l\zeta_5$ [Figs. 2(a) and (b)], the evaporative cooling of the liquid-vapor interface leads to a negative thermal gradient along the normal direction toward the interface. Although for both systems “small-on-top” stratification is expected by the model of Zhou *et al.* since $Pe_l \gg Pe_s > 1$,[20] thermophoresis associated with the negative temperature gradient works against diffusiophoresis and transports more LNPs into the interfacial region. As a result, the two systems exhibit “large-on-top” stratification.

When all the solvent beads in the simulation cell are thermalized during evaporation, the temperature in the entire system is constant and no thermal gradients are produced. Thermophoresis is thus suppressed and only diffusiophoresis remains. The expected outcome is “small-on-top” stratification for $Pe_l \gg Pe_s > 1$. The results from $T_{1.0}\zeta_{30}$ and $T_{1.0}\zeta_5$ confirm this prediction, as shown in Figs. 2(c) and (d). For example, comparing the last snapshot for $T_{1.0}^l\zeta_5$ (the second row of Fig. 2) and that for $T_{1.0}\zeta_5$ (the fourth row of Fig. 2), the transition from “large-on-top” to “small-on-top” is clearly visible after the thermal gradients and the associated thermophoresis are inhibited.

The last row of Fig. 2 shows the snapshots for $T_{1.0}^lT_{1.2}^v\zeta_5$. In this system, the vapor beads of the solvent at $\sim 23\sigma$ above the initial liquid-vapor interface prior to evaporation are thermalized at $T_v = 1.2\epsilon/k_B > T_l$

TABLE I. Parameters for all the systems studied. Refer to Fig. 1 for the thermalization schemes.

System	ζ	$v_e\tau/\sigma$	Pe_l	Pe_s	Thermalization Scheme
$T_{1.0}^l\zeta_{30}$	30	1.13×10^{-3}	195.4	22.2	A
$T_{1.0}^l\zeta_5$	5	2.04×10^{-4}	35.3	4.0	A
$T_{1.0}\zeta_{30}$	30	1.18×10^{-3}	204.4	23.2	B
$T_{1.0}\zeta_5$	5	2.11×10^{-4}	36.6	4.1	B
$T_{1.0}^lT_{1.2}^v\zeta_5$	5	2.04×10^{-4}	35.3	4.0	C, $T_v = 1.2\epsilon/k_B$
$T_{1.0}^lT_{1.1}^v\zeta_5$	5	1.99×10^{-4}	34.4	3.9	C, $T_v = 1.1\epsilon/k_B$
$T_{1.0}^lT_{1.05}^v\zeta_5$	5	2.04×10^{-4}	35.3	4.0	C, $T_v = 1.05\epsilon/k_B$
$T_{1.0}^lT_{0.9}^v\zeta_5$	5	6.93×10^{-4}	119.7	13.6	C, $T_v = 0.9\epsilon/k_B$
$T_{1.0}^lT_{0.85}^v\zeta_5$	5	9.90×10^{-4}	171.0	19.4	C, $T_v = 0.85\epsilon/k_B$
$T_{1.0}^lT_{0.75}^v\zeta_5$	5	1.03×10^{-3}	177.2	20.2	C, $T_v = 0.75\epsilon/k_B$

during evaporation. The top region of the drying suspension is thus heated. Consequently, there is a positive temperature gradient in the liquid solvent along the normal direction toward the interface. The solvent density develops a negative gradient and the accompanied thermophoresis drives LNPs toward the substrate. As a result, thermophoretic and diffusiophoretic effects are in synergy and strong “small-on-top” stratification is generated, which is apparent in Fig. 2(e).

To understand quantitatively the stratifying phenomena in drying particle suspensions, we plot the temperature and density profiles in Fig. 3. The local temperature $T(z)$ at height z is computed from the average kinetic energy of the solvent beads in the spatial bin $[z - 2.5\sigma, z + 2.5\sigma]$. [42] The temperature profiles in the top row of Fig. 3 clearly show the negative thermal gradients induced by evaporative cooling for $T_{1.0}^l\zeta_{30}$ and $T_{1.0}^l\zeta_5$, with the effect stronger at larger evaporation rates. $T_{1.0}\zeta_{30}$ and $T_{1.0}\zeta_5$ do not exhibit thermal gradients as all the solvent is thermalized at T_l , as shown in Figs. 3(i) and (m). $T_{1.0}^lT_{1.2}^v\zeta_5$ with $T_v > T_l$ exhibits an externally imposed positive thermal gradient [Fig. 3(q)].

The local density of solvent or nanoparticles is computed as $\rho_i(z) = n_i(z)m_i/(L_xL_y\sigma)$, where $n_i(z)$ represents the number of particles in the spatial bin $[z - 0.5\sigma, z + 0.5\sigma]$ and m_i is the particle mass. A nanoparticles straddling several bins is partitioned based on its partial volume in each bin. When computing the solvent density, the volume occupied by the nanoparticles is subtracted. The second row of Fig. 3 shows the solvent density as a function of height and the profiles exhibit gradients in accordance with the thermal gradients. Particularly, a positive (negative) thermal gradient generates a negative (positive) density gradient for the solvent and the stronger the thermal gradient, the stronger the density gradient. This correlation results from the fact that local thermal equilibrium is always maintained even at the fastest evaporation rates adopted in our simulations. [42]

The density profiles for LNPs and SNPs are shown in the bottom two rows of Fig. 3, respectively. These profiles demonstrate the phoretic response of the nanopar-

ticles to the thermal gradients (or the density gradients of the solvent induced by the thermal gradients) as well as the effects of the evaporation rate. For all the simulations discussed here, the evaporation rates are high enough such that $Pe_l \gg Pe_s > 1$. The corresponding fast receding liquid-vapor interface tends to trap both LNPs and SNPs just below the interface. If no other factors are at play, this effect combined with a large enough ϕ_s is expected to yield “small-on-top” stratification via the diffusiophoresis mechanism as suggested by Sear and collaborators [18, 25] and Zhou *et al.* [20] This scenario is indeed the case for $T_{1.0}\zeta_{30}$ and $T_{1.0}\zeta_5$, as shown in the third and fourth columns of Fig. 3 where there are no thermal gradients. The diffusiophoresis model also implies that the degree of “small-on-top” stratification is enhanced when the evaporation rate is increased. [18, 20] However, as shown later, $T_{1.0}\zeta_5$ actually exhibits stronger “small-on-top” stratification than $T_{1.0}\zeta_{30}$, even though the evaporation rate is increased six fold in the latter system. This discrepancy may be due to the small thickness of the suspension film studied in our simulations, which is limited by the available computational resources. The effect of film thickness on stratification will be explored in the future.

When only a thin layer of solvent beads at the bottom wall is thermalized, the temperature in the vicinity of the liquid-vapor interface decreases because of evaporative cooling effect. The resulting enhancement of the solvent density at the interface leads to thermophoretic drift of nanoparticles with the effect more significant for larger particles. This physical picture explains the observations for $T_{1.0}^l\zeta_{30}$ and $T_{1.0}^l\zeta_5$. In these two systems, the SNPs are found to accumulate at the surface of the evaporating suspension as $Pe_l \gg Pe_s > 1$ [Figs. 3(d) and (h)]. However, a significant accumulation of LNPs is found just below the enriched surface layer of SNPs, as shown in Figs. 3(c) and (g). The net outcome is actually “large-on-top” stratification, which will be confirmed later with an order parameter quantifying stratification (see Fig. 4). Furthermore, the degree of “large-on-top” stratification is stronger for $T_{1.0}^l\zeta_5$ than for $T_{1.0}^l\zeta_{30}$, indicating a delicate competition between diffusiophoresis and thermophore-

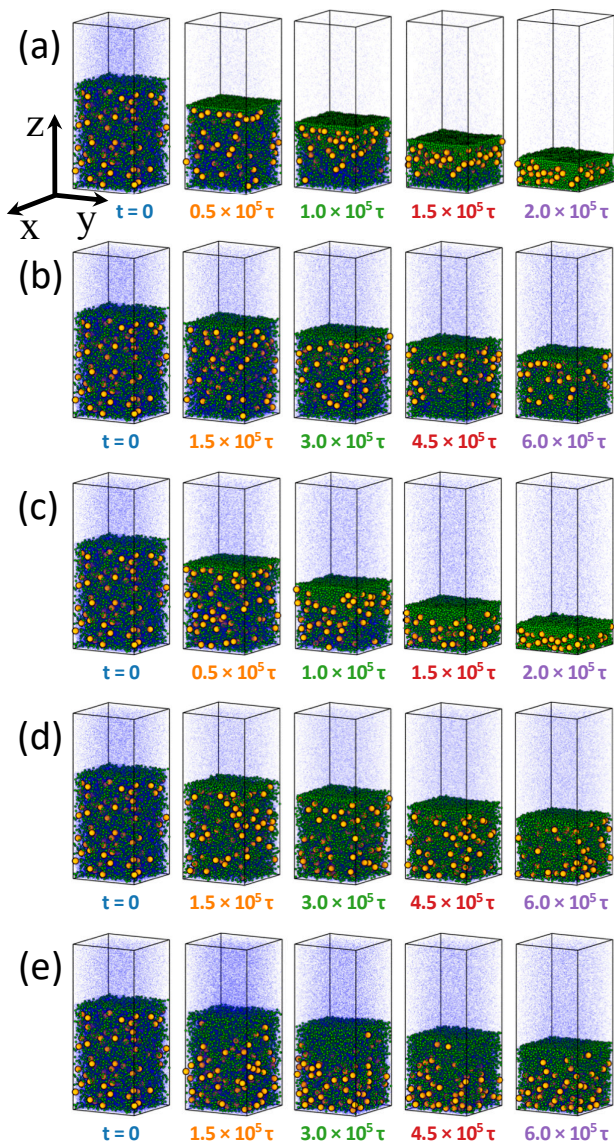


FIG. 2. Snapshots during solvent evaporation for (a) $T_{1.0}^l \zeta_{30}$, (b) $T_{1.0}^l \zeta_5$, (c) $T_{1.0} \zeta_{30}$, (d) $T_{1.0} \zeta_5$, and (e) $T_{1.0}^l T_{1.2}^v \zeta_5$. Elapsed time since evaporation was initiated at $t = 0$ is listed under each snapshot. Temperature and density profiles of the five systems are shown in Fig. 3. Color code: SNPs (green), LNPs (orange), and solvent (blue). Only 5% of the solvent beads are visualized to improve clarity.

sis. The lower evaporation rate in $T_{1.0}^l \zeta_5$ suppresses both processes but it appears that diffusiophoresis is mitigated slightly more, creating stronger “large-on-top” for $T_{1.0}^l \zeta_5$.

In our previous work,[30] we obtained a state diagram of stratification with systems all thermalized with Scheme A (i.e., a thin layer of liquid solvent contacting the substrate is thermalized at $T_l = 1.0\epsilon/k_B$) and only observed weak “small-on-top” stratification at values of Pe_s and ϕ_s far exceeding the critical values predicted the diffusiophoretic model of Zhou *et al.*[20] The presence of thermophoresis at fast evaporation rates may help understand the discrepancy between the simulations

and the theory.[30] Indeed, when thermophoresis is suppressed, systems that are driven into the “large-on-top” regime by thermophoresis can be turned into (usually weak) “small-on-top”. Examples are the transition from $T_{1.0}^l \zeta_{30}$ to $T_{1.0} \zeta_{30}$ and that from $T_{1.0}^l \zeta_5$ to $T_{1.0} \zeta_5$.

To achieve strong “small-on-top” stratification, a natural idea is to enable thermophoresis that works in conjunction with diffusiophoresis. This cooperation requires a thermal gradient during evaporation that is opposite to the one induced by evaporative cooling. To realize this, we thermalize the vapor zone from $L_z - 150\sigma$ to L_z at a temperature $T_v > T_l$. The data in the fifth column of Fig. 3 are for $T_{1.0}^l T_{1.2}^v \zeta_5$ where $T_v = 1.2\epsilon/k_B$. A positive thermal gradient and a negative density gradient of the solvent can be seen clearly in Figs. 3(q) and (r), respectively. Since the gradients are reversed, the LNPs are now driven toward the substrate via thermophoresis [Fig. 3(s)] while the SNPs are much less affected [Fig. 3(t)]. The final result is strong “small-on-top” stratification where the LNPs are accumulated near the substrate and depleted in the interfacial region while the SNPs exhibit a positive density gradient (i.e., accumulation) toward the interface.

It is expected that for systems thermalized with Scheme C and $T_v < T_l$, a negative thermal gradient develops in the liquid solvent, similar to the evaporative cooling case in Scheme A. Consequently, systems under Scheme C with $T_v < T_l$ could display “large-on-top” stratification as long as the thermal gradient is large enough. These cases are in fact observed and discussed in detail in the Supporting Information, where some complications are noted related to droplet condensation in a vapor that is thermalized at low temperatures.

To quantify stratification, we define an order parameter using the full density profiles of nanoparticles.[30] The mean heights of LNPs and SNPs are computed as $\langle z_i \rangle = \frac{1}{N_i} \sum_{n=1}^{N_i} z_{in}$ with $i \in \{l, s\}$. The order parameter of stratification is then computed as $(2\langle z_l \rangle - 2\langle z_s \rangle)/H(t)$, i.e., the mean separation between LNPs and SNPs normalized by $H(t)/2$, where $H(t)$ is the instantaneous thickness of the suspension. In the equilibrium suspension prior to evaporation, both $\langle z_l \rangle$ and $\langle z_s \rangle$ are very close to $H(0)/2$, where $H(0)$ is the initial film thickness. During evaporation, $\langle z_l \rangle - \langle z_s \rangle < 0$ indicates “small-on-top” stratification while $\langle z_l \rangle - \langle z_s \rangle > 0$ signifies “large-on-top”.

In Fig. 4 the order parameter of stratification is plotted against the extent of drying, quantified as $(H(0) - H(t))/H(0)$, for the first five systems listed in Table I. It is clear that $T_{1.0} \zeta_{30}$ and $T_{1.0} \zeta_5$ exhibit “small-on-top” stratification when diffusiophoresis dominates while thermal gradients and thermophoresis are absent. The extent of stratification is slightly stronger for $T_{1.0} \zeta_5$, though it dries more slowly. “Large-on-top” is observed for $T_{1.0}^l \zeta_{30}$ and $T_{1.0}^l \zeta_5$ and is again stronger for $T_{1.0}^l \zeta_5$ that has a smaller evaporation rate. Although thermophoresis is much weaker for $T_{1.0}^l \zeta_5$ because of the reduced evaporation rate, diffusiophoresis favoring “small-on-top” is sup-

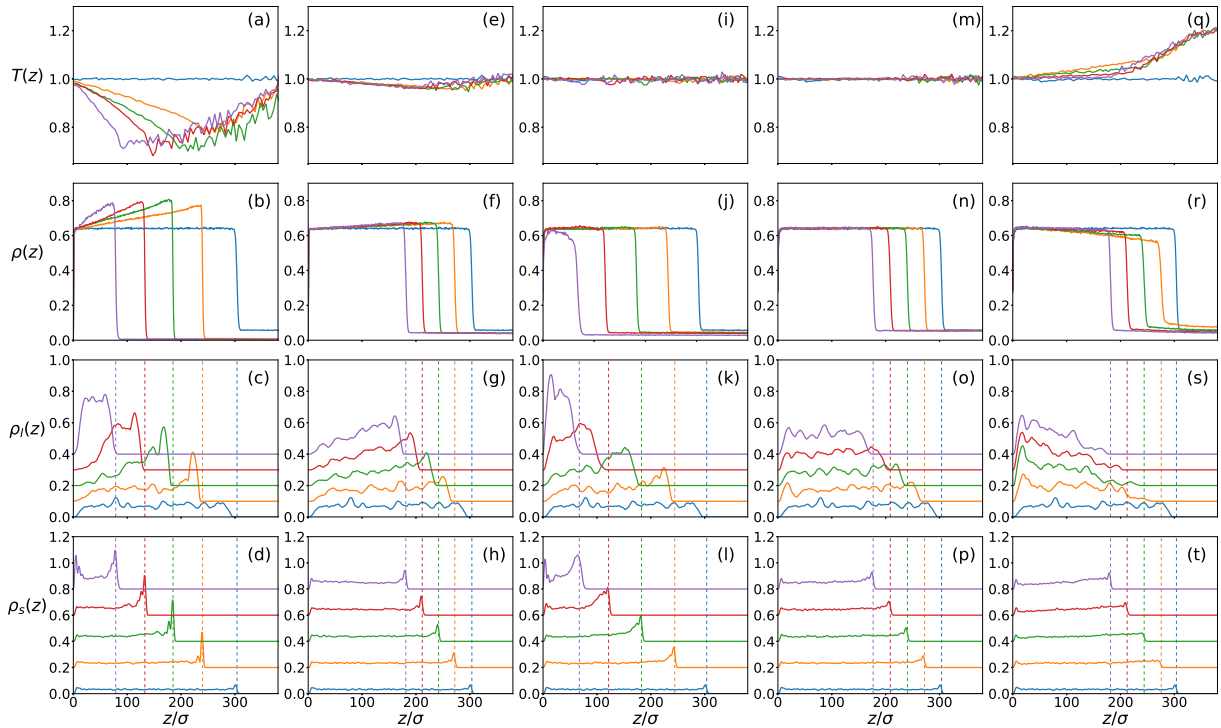


FIG. 3. Temperature profiles (top row) and density profiles for the solvent (second row), LNPs (third row), and SNPs (bottom row) for $T_{1.0}^l \zeta_{30}$ (a-d), $T_{1.0}^l \zeta_5$ (e-h), $T_{1.0}^l \zeta_{30}$ (i-l), $T_{1.0}^l \zeta_5$ (m-p), and $T_{1.0}^l T_{1.2}^v \zeta_5$ (q-t), respectively. The curves follow the same order as the snapshots shown Fig. 2. The vertical dashed lines indicate the location of the liquid-vapor interface. For clarity, the density profiles for LNPs (SNPs) are shifted upward by $0.1m/\sigma^3$ ($0.2m/\sigma^3$) successively.

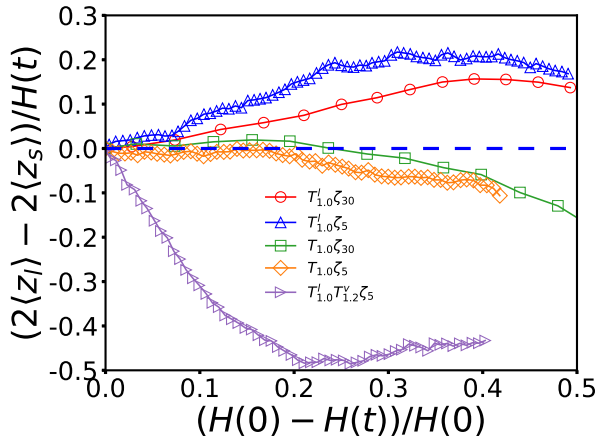


FIG. 4. Mean separation between LNPs and SNPs normalized by $H(t)/2$, vs extent of drying, $(H(0) - H(t))/H(0)$, for $T_{1.0}^l \zeta_{30}$ (red circle), $T_{1.0}^l \zeta_5$ (blue upward triangle), $T_{1.0}^l \zeta_{30}$ (green square), $T_{1.0}^l \zeta_5$ (yellow diamond), and $T_{1.0}^l T_{1.2}^v \zeta_5$ (purple right-pointing triangle).

pressed even more when evaporation is slowed down and the delicate interplay of the two phoretic processes leads to stronger “large-on-top” stratification for $T_{1.0}^l \zeta_5$.

A dramatic “small-on-top” state is clearly demonstrated in Fig. 4 for $T_{1.0}^l T_{1.2}^v \zeta_5$. Note that in the equi-

librium suspension, $\phi_l = 2\phi_s$. If in the final dry film all the SNPs were on top of all the LNPs (i.e., a complete stratification) but each group is uniformly distributed in its region, then $\langle z_l \rangle = H(t)/3$ and $\langle z_s \rangle = 5H(t)/6$, yielding $(2\langle z_l \rangle - 2\langle z_s \rangle)/H(t) = -1$. As shown in Fig. 4, the order parameter of stratification reaches a minimal value around -0.5 for $T_{1.0}^l T_{1.2}^v \zeta_5$, indicating that the vertical distribution of the binary mixture of nanoparticles is substantially segregated in the drying film with SNPs on top of LNPs. This outcome is clearly visible in Fig. 2(e) as well.

Evaporative cooling is a natural effect in a fast drying liquid. If a particle suspension is placed on a substrate that is kept at a constant temperature and the suspension undergoes very fast solvent evaporation, then a temperature lower than that of the substrate is expected at the evaporating interface, resulting in a negative thermal gradient in the suspension. $T_{1.0}^l \zeta_{30}$ and $T_{1.0}^l \zeta_5$ studied here are set up to mimic such situations. However, it is challenging to maintain a constant temperature or induce a positive thermal gradient along the normal direction toward the interface in a drying suspension, especially when the evaporation rate is high. One possible approach is to dissolve a gas (e.g., N_2 , Ar, He, or CO_2) into the solvent (e.g., water). Beaglehole showed that heating a water film with a dissolved gas from above or below produces very different temperature distributions within the

liquid.[43, 44] When heated from below, a fairly uniform temperature is found throughout the liquid. However, when the liquid is heated from above, a temperature gradient develops in it with the temperature higher at the liquid-vapor interface. Then it may be possible to study the effect of solvent evaporation on the particle distribution in a drying film under isothermal conditions and positive thermal gradients, similar to Scheme B and C.

IV. CONCLUSIONS

In this paper we focus on how stratification can be controlled in a drying suspension of a bidisperse mixture of nanoparticles via MD simulations with an explicit solvent model. We demonstrate that a thermal gradient and the induced thermophoresis can be used to alter stratification from “large-on-top” all the way to strong “small-on-top”. This strategy is based on the observation that particles of different sizes in a suspension have different responses to a thermal gradient. In particular, larger particles experience a larger driving force that transports them into cooler regions where the solvent density is higher. For $A_{\text{ns}} = 100\epsilon$ adopted here, the smaller nanoparticles show little or even no response to a thermal gradient. When a suspension undergoes fast drying and only a thin layer of the solvent adjacent to the substrate is thermalized at T_l , mimicking an experimental situation where the substrate supporting the suspension is maintained at a constant temperature during solvent evaporation, a negative temperature gradient develops in the suspension because of the evaporative cooling effect that makes the temperature at the evaporating interface to drop below T_l . A larger fraction of the larger nanoparticles are driven into the interfacial region via the thermophoresis induced by this thermal gradient. As a result, the fast drying suspensions display “large-on-top” stratification instead of “small-on-top” expected by the diffusiophoresis model in which the suspension is assumed to be isothermal during evaporation.

Interestingly, when the entire suspension is maintained at T_l during drying by thermalizing all the solvent beads

in the simulation cell, they do exhibit “small-on-top” stratification at fast evaporation rates, consistent with the prediction of the diffusiophoresis model.[18, 20, 25] However, the degree of stratification is found to be weak, probably due to the fact that ϕ_s is small and the liquid film is thin for the simulations reported here. When a positive thermal gradient is induced in the suspension by thermalizing the vapor at a temperature higher than T_l , all the larger nanoparticles are propelled toward the substrate. In this case, the synergy between thermophoresis and diffusiophoresis is underlying the observation of strong “small-on-top” stratification. Our results thus reveal a potentially useful strategy of controlling stratification via a regulated thermal gradient in a drying suspension of polydisperse particles.

ACKNOWLEDGEMENT

Acknowledgment is made to the Donors of the American Chemical Society Petroleum Research Fund (PRF #56103-DNI6), for support of this research. This research used resources of the National Energy Research Scientific Computing Center (NERSC), a U.S. Department of Energy Office of Science User Facility operated under Contract No. DE-AC02-05CH11231. These resources were obtained through the Advanced Scientific Computing Research (ASCR) Leadership Computing Challenge (ALCC). This work was performed, in part, at the Center for Integrated Nanotechnologies, an Office of Science User Facility operated for the U.S. Department of Energy Office of Science. Sandia National Laboratories is a multimission laboratory managed and operated by National Technology and Engineering Solutions of Sandia, LLC., a wholly owned subsidiary of Honeywell International, Inc., for the U.S. Department of Energy’s National Nuclear Security Administration under contract DE-NA0003525. This paper describes objective technical results and analysis. Any subjective views or opinions that might be expressed in the paper do not necessarily represent the views of the U.S. Department of Energy or the United States Government.

-
- [1] D. P. Sheetz, *J. Appl. Polym. Sci.* **9**, 3759 (1965).
 - [2] J. L. Keddie, *Mater. Sci. Engr. R: Reports* **21**, 101 (1997), ISSN 0927-796X.
 - [3] P. Steward, J. Hearn, and M. Wilkinson, *Adv. Colloid Interface Sci.* **86**, 195 (2000), ISSN 0001-8686.
 - [4] W. B. Russel, *AIChE J.* **57**, 1378 (2011).
 - [5] A. F. Routh, *Rep. Prog. Phys.* **76**, 046603 (2013).
 - [6] J. Zhou, X. Man, Y. Jiang, and M. Doi, *Adv. Mater.* **29**, 1703769 (2017).
 - [7] M. Schulz and J. L. Keddie, *Soft Matter* **14**, 6181 (2018).
 - [8] R. A. Cairncross, L. F. Francis, and L. E. Scriven, *AIChE J.* **42**, 55 (1996).
 - [9] A. F. Routh and W. B. Zimmerman, *Chem. Eng. Sci.* **59**, 2961 (2004).
 - [10] C. M. Cardinal, Y. D. Jung, K. H. Ahn, and L. F. Francis, *AIChE J.* **56**, 2769 (2010).
 - [11] I. Nikiforow, J. Adams, A. M. König, A. Langhoff, K. Pohl, A. Turshatov, and D. Johannsmann, *Langmuir* **26**, 13162 (2010).
 - [12] R. E. Trueman, E. Lago Domingues, S. N. Emmett, M. W. Murray, and A. F. Routh, *J. Colloid Interface Sci.* **377**, 207 (2012).
 - [13] R. E. Trueman, E. Lago Domingues, S. N. Emmett, M. W. Murray, J. L. Keddie, and A. F. Routh, *Langmuir* **28**, 3420 (2012).

- [14] A. K. Atmuri, S. R. Bhatia, and A. F. Routh, *Langmuir* **28**, 2652 (2012).
- [15] S. Cheng and G. S. Grest, *J. Chem. Phys.* **138**, 064701 (2013).
- [16] F. Doumenc, J.-B. Salmon, and B. Guerrier, *Langmuir* **32**, 13657 (2016).
- [17] M. P. Howard, W. F. Reinhart, T. Sanyal, M. S. Shell, A. Nikoubashman, and A. Z. Panagiotopoulos, *J. Chem. Phys.* **149**, 094901 (2018).
- [18] A. Fortini, I. Martín-Fabiani, J. L. De La Haye, P.-Y. Dugas, M. Lansalot, F. D'Agosto, E. Bourgeat-Lami, J. L. Keddie, and R. P. Sear, *Phys. Rev. Lett.* **116**, 118301 (2016).
- [19] I. Martín-Fabiani, A. Fortini, J. Lesage de la Haye, M. L. Koh, S. E. Taylor, E. Bourgeat-Lami, M. Lansalot, F. D'Agosto, R. P. Sear, and J. L. Keddie, *ACS Appl. Mater. Interfaces* **8**, 34755 (2016).
- [20] J. Zhou, Y. Jiang, and M. Doi, *Phys. Rev. Lett.* **118**, 108002 (2017).
- [21] A. Fortini and R. P. Sear, *Langmuir* **33**, 4796 (2017).
- [22] M. P. Howard, A. Nikoubashman, and A. Z. Panagiotopoulos, *Langmuir* **33**, 3685 (2017).
- [23] M. P. Howard, A. Nikoubashman, and A. Z. Panagiotopoulos, *Langmuir* **33**, 11390 (2017).
- [24] D. K. Makepeace, A. Fortini, A. Markov, P. Locatelli, C. Lindsay, S. Moorhouse, R. Lind, R. P. Sear, and J. L. Keddie, *Soft Matter* **13**, 6969 (2017).
- [25] R. P. Sear and P. B. Warren, *Phys. Rev. E* **96**, 062602 (2017).
- [26] R. P. Sear, *J. Chem. Phys.* **148**, 134909 (2018).
- [27] X. Liu, W. Liu, A. J. Carr, D. S. Vazquez, D. Nykypanchuk, P. W. Majewski, A. F. Routh, and S. R. Bhatia, *J. Colloid Interface Sci.* **515**, 70 (2018), ISSN 0021-9797.
- [28] R. Tatsumi, T. Iwao, O. Koike, Y. Yamaguchi, and Y. Tsuji, *Appl. Phys. Lett.* **112**, 053702 (2018), ISSN 00036951.
- [29] O. Cusola, S. Kivistö, S. Vierros, P. Batys, M. Ago, B. L. Tardy, L. G. Greca, M. B. Roncero, M. Sammalkorpi, and O. J. Rojas, *Langmuir* **34**, 5759 (2018).
- [30] Y. Tang, G. S. Grest, and S. Cheng, *Langmuir* **34**, 7161 (2018), ISSN 15205827.
- [31] A. J. Carr, W. Liu, K. G. Yager, A. F. Routh, and S. R. Bhatia, *ACS Appl. Nano Mater.* **1**, 4211 (2018).
- [32] A. Statt, M. P. Howard, and A. Z. Panagiotopoulos, *J. Chem. Phys.* **149**, 024902 (2018).
- [33] I. Martín-Fabiani, M. L. Koh, F. Dalmas, K. L. Elidottir, S. J. Hinder, I. Jurewicz, M. Lansalot, E. Bourgeat-Lami, and J. L. Keddie, *ACS Appl. Nano Mater.* **1**, 3956 (2018).
- [34] A. F. Routh and W. B. Russel, *AIChE J.* **44**, 2088 (1998).
- [35] R. Everaers and M. R. Ejtehadi, *Phys. Rev. E* **67**, 041710 (2003).
- [36] P. J. in 't Veld, S. J. Plimpton, and G. S. Grest, *Comput. Phys. Commun.* **179**, 320 (2008).
- [37] S. Cheng and G. S. Grest, *J. Chem. Phys.* **136**, 214702 (2012).
- [38] P. J. in 't Veld, M. K. Petersen, and G. S. Grest, *Phys. Rev. E* **79**, 021401 (2009).
- [39] S. Plimpton, *J. Comput. Phys.* **117**, 1 (1995).
- [40] R. Piazza and A. Parola, *J. Phys. Condens. Matter* **20**, 153102 (2008), ISSN 09538984.
- [41] H. Brenner, *Phys. Rev. E* **84**, 066317 (2011).
- [42] S. Cheng, J. B. Lechman, S. J. Plimpton, and G. S. Grest, *J. Chem. Phys.* **134**, 224704 (2011).
- [43] D. Beaglehole, *J. Phys. Chem.* **91**, 5091 (1987).
- [44] V. Kuz, A. Garazo, and S. Fasano, *J. Colloid Interface Sci.* **133**, 511 (1989), ISSN 0021-9797.

SUPPORTING INFORMATION

Diffusion Coefficients of Nanoparticles:

The diffusion coefficients of the large nanoparticles (LNPs) and small nanoparticles (SNPs) were determined by an independent simulation. A suspension of LNPs and SNPs with the same volume fractions as in the initial suspension discussed in the main text, but without the vapor phase of the solvent, was prepared. The suspension has a cubic shape with edge length 101.3σ . Periodic boundary conditions were used in all three directions. The mean square displacements of both LNPs and SNPs as a function of time are shown in Fig. S1. The data show a clear transition from ballistic regime at short times to diffusive regime at long times. The diffusion coefficients are $D_l = 1.76 \times 10^{-3} \sigma^2/\tau$ for LNPs and $D_s = 1.55 \times 10^{-2} \sigma^2/\tau$ for SNPs.

Thermophoresis of Nanoparticles:

To understand the thermophoresis of nanoparticles, we performed additional simulations for suspensions of only SNPs or only LNPs at volume fractions close to those in the suspension of the mixture of SNPs and LNPs. Each suspension was first equilibrated at $T = 1.0\epsilon/k_B$. Then a thermal gradient was introduced into the system by thermalizing a top region of the liquid solvent and all the vapor at $T_H = 1.0\epsilon/k_B$ while thermalizing a layer of the solvent adjacent to the bottom wall at T_L , as shown in Fig. S2. Two values of T_L , $0.9\epsilon/k_B$ and $0.7\epsilon/k_B$, were used to generate a thermal gradient with different magnitudes in the direction perpendicular to the liquid-vapor interface. The average position of nanoparticles in each system was recorded as a function of time after the thermal gradient was imposed and the data are plotted in Fig. S3. Since T_L is lower than the initial temperature of the equilibrium suspension, the liquid contracts and the liquid-vapor interface recedes when the thermal gradient is imposed. Our data show that for the nanoparticle-solvent interaction with $A_{ns} = 100\epsilon$, the SNPs first move toward the substrate because of the contraction of the liquid solvent. After this transient phase, the SNPs do not show any response to the imposed thermal gradient and their average position remains almost constant with time. However, the LNPs show a clear thermophoretic response to the thermal gradient and drift toward the cooler region where the liquid density is higher. These independent simulations thus demonstrate that for the parameters used in this paper, the LNPs exhibit strong thermophoresis while the SNPs exhibit none.

Additional Simulations and Results:

We ran 5 additional simulations in which the systems were thermalized with Scheme C with $T_l = 1.0\epsilon/k_B$ and $T_v = 1.1\epsilon/k_B$, $1.05\epsilon/k_B$, $0.9\epsilon/k_B$, $0.85\epsilon/k_B$, and $0.75\epsilon/k_B$ at an evaporation rate set by $\zeta = 5$, as listed in Table 1 of the main text. Snapshots at various times during evaporation are shown in Fig. S4 for $T_{1.0}^l T_{1.1}^v \zeta_5$, $T_{1.0}^l T_{1.05}^v \zeta_5$, and $T_{1.0}^l T_{0.75}^v \zeta_5$. The corresponding temperature and density profiles for these 3 systems are shown in Fig. S5. The results for $T_{1.0}^l T_{0.85}^v \zeta_5$ and $T_{1.0}^l T_{0.9}^v \zeta_5$ are similar to those for $T_{1.0}^l T_{0.75}^v \zeta_5$.

Similar to $T_{1.0}^l T_{1.2}^v \zeta_5$, $T_{1.0}^l T_{1.1}^v \zeta_5$ exhibits “small-on-top” stratification, though it is difficult to see this behavior clearly from the snapshots in Fig. S4(a). For this system, there is a weak positive thermal gradient in the evaporating suspension toward the liquid-vapor interface [Fig. S5(a)]. Via the thermophoresis induced by this gradient, the LNPs are driven toward the substrate (i.e., toward the bottom of the liquid film) and depleted near the liquid-vapor interface. This depletion almost balances the accumulation of LNPs near the top of the film caused by the fast receding interface. As a result, the LNPs are almost uniformly distributed in the drying film, as shown in Figs. S5(c) and S6(a). The SNPs are essentially unaffected by the thermal gradient and accumulate below the interface since $Pe_s > 1$ [see Figs. S5(d) and S6(b)]. The net outcome is “small-on-top” stratification for $T_{1.0}^l T_{1.1}^v \zeta_5$, as shown by the order parameter of stratification plotted in Fig. S6(c).

For $T_{1.0}^l T_{1.05}^v \zeta_5$, the evaporative cooling in the solvent is balanced by the heating from the vapor thermalized at $T_v = 1.05\epsilon/k_B$. The temperature and solvent density are almost uniform in the evaporating suspension, as shown in Figs. S5(e) and S5(f). Both LNPs and SNPs accumulate below the receding interface as $Pe_1 > Pe_s > 1$ [see Figs. S5(g) and S5(h) and Figs. S6(a) and S6(b)]. The distribution of nanoparticles in this system does not stratify in the early stage of drying, though there is a transition to weak “large-on-top” at late times, as shown by the corresponding order parameter of stratification in Fig. S6(c).

$T_{1.0}^l T_{1.2}^v \zeta_5$ has been discussed in detail in the main text. Fig. S6 shows the results of the average position of nanoparticles normal to the interface and the order parameter of stratification for $T_{1.0}^l T_{1.2}^v \zeta_5$, $T_{1.0}^l T_{1.1}^v \zeta_5$, and $T_{1.0}^l T_{1.05}^v \zeta_5$. This comparison clearly shows the transition from strong to weak “small-on-top” stratification and finally to almost no stratification or weak “large-on-top” when $T_v - T_l$ is reduced.

$T_{1.0}^l \zeta_5$ has a weak negative thermal gradient in the evaporating suspension because of evaporative cooling. Via the associated thermophoretic process, the LNPs are pushed toward the liquid-vapor interface where the solvent density is higher. Thermophoresis overpowers diffusiophoresis where the LNPs are pushed away from the interface by the concentration gradient of the SNPs. As a result, $T_{1.0}^l \zeta_5$ exhibits “large-on-top” stratification. Motivated by this observation, we ran $T_{1.0}^l T_{0.75}^v \zeta_5$ that has a large $|T_v - T_l|$. Our original goal was to induce a large negative thermal gradient in the evaporating suspension at a relatively small v_s such that the accompanying thermophoresis could generate strong “large-on-top” stratification in the drying suspension. However, as the initial vapor phase is at

equilibrium with a liquid at $T_l = 1.0\epsilon/k_B$, cooling the vapor down to $T_v = 0.75\epsilon/k_B$ leads to droplet condensation in the vapor phase, as shown in Fig. S4(c). Eventually, a liquid film of the solvent beads is formed at the top of the simulation cell. Because of the condensation, the vapor density near the liquid-vapor interface decreases very quickly and as a result, the solvent evaporates at a rate much higher than for $\zeta = 5$. The actual evaporation rate in $T_{1.0}^l T_{0.75}^v \zeta_5$ is close to that in $T_{1.0}^l \zeta_{30}$. Increasing T_v to $0.85\epsilon/k_B$ or $0.90\epsilon/k_B$ yields similar droplet condensation in the vapor phase, though the extent of condensation decreases as T_v is increased. As a result, the receding speed of the liquid-vapor interface during evaporation decreases and becomes closer from above to the value set by $\zeta = 5$.

The average positions of LNPs and SNPs during drying are plotted in Fig. S7 as a function of the extent of drying for the 5 systems discussed in the main text (see Table 1), as well as $T_{1.0}^l T_{0.75}^v \zeta_5$. It is clear that the LNPs have a large thermophoretic response while the SNPs only show changes in their average position in the late stage of drying, when the thermal gradient is varied. The behavior of SNPs is predominately affected by the receding speed of the liquid-vapor interface. The variation of their average positions in the late stage of drying under different thermal gradients is due to the change in the distribution of LNPs in the drying film. For example, when the LNPs are concentrated in a region, the SNPs are driven out of the same region because of crowding.

In Fig. S8, the order parameter of stratification is plotted as a function of the extent of drying for $T_{1.0}^l \zeta_{30}$, $T_{1.0}^l \zeta_5$, and $T_{1.0}^l T_{0.75}^v \zeta_5$. $T_{1.0}^l T_{0.75}^v \zeta_5$ exhibits “large-on-top” stratification with an amplitude very close to that in $T_{1.0}^l \zeta_{30}$ for reasons discussed previously. The reason that $T_{1.0}^l \zeta_5$ shows even stronger “large-on-top” stratification than $T_{1.0}^l \zeta_{30}$ is discussed in the main text.

In Fig. S9, we plot the average position of nanoparticles and the average separation between LNPs and SNPs for the 3 systems with $T_v < T_l$, i.e., $T_{1.0}^l T_{0.75}^v \zeta_5$, $T_{1.0}^l T_{0.85}^v \zeta_5$, and $T_{1.0}^l T_{0.9}^v \zeta_5$. While the SNPs show very little response to a thermal gradient, the distribution of LNPs is sensitive to the strength of the thermal gradient. When T_v approaches T_l from below, the negative thermal gradient in the evaporating suspension becomes smaller in magnitude and the driving force for LNPs to migrate to the interfacial region decreases. However, the receding speed of the liquid-vapor interface also decreases as T_v is increased and gets closer to T_l from below, and the diffusiophoretic driving force that pushes LNPs way from the interfacial region thus decreases. The complicated interplay of these two factors makes “large-on-top” stratification stronger when T_v is increased as in $T_{1.0}^l T_{0.75}^v \zeta_5 \rightarrow T_{1.0}^l T_{0.85}^v \zeta_5 \rightarrow T_{1.0}^l T_{0.9}^v \zeta_5$ [see Fig. S9(c)].

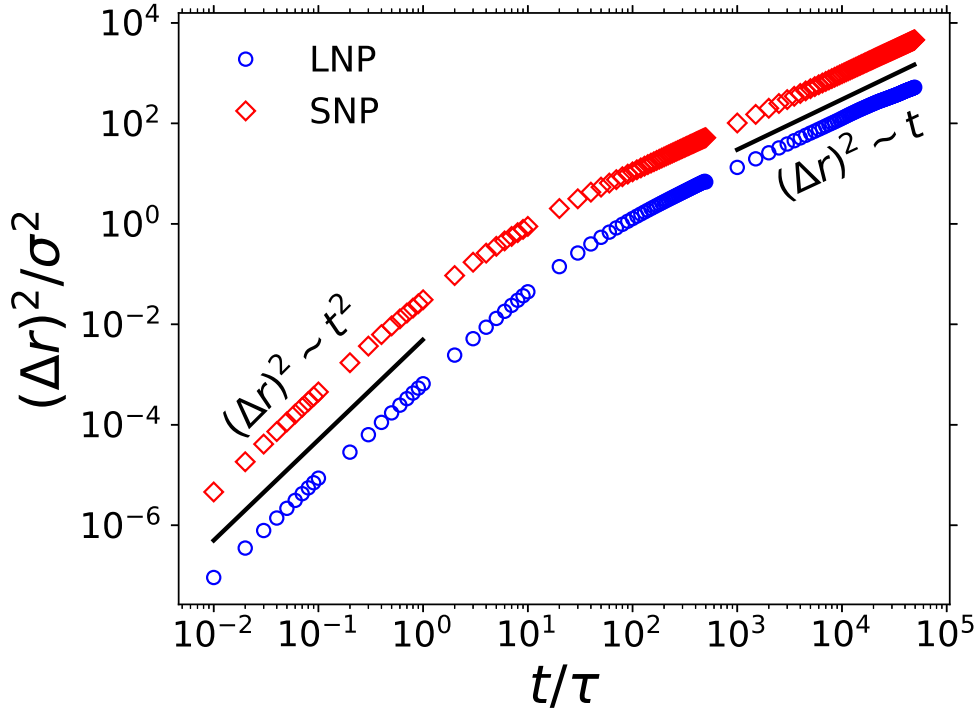


FIG. S1. Mean square displacement *vs* time for LNPs (blue circles) and SNPs (red diamonds).

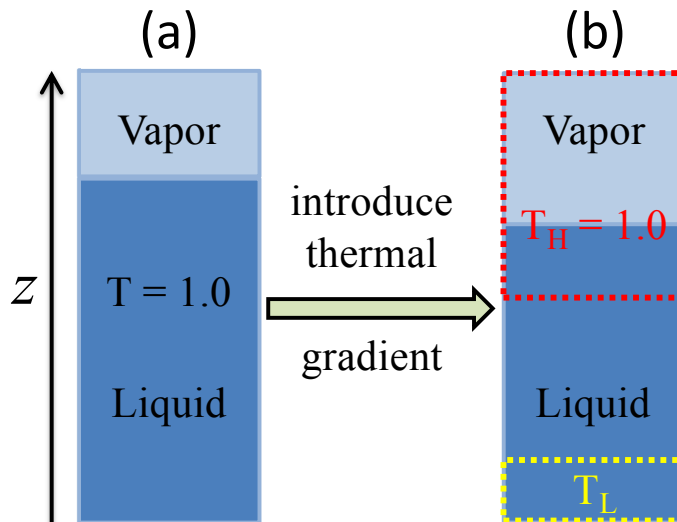


FIG. S2. The simulation set-up to study thermophoresis: (a) the entire solvent and vapor are thermalized at $T = 1.0\epsilon/k_B$; (b) a top region of the liquid solvent and all the vapor are thermalized at $T_H = 1.0\epsilon/k_B$ while a layer of the solvent adjacent to the bottom wall is thermalized at T_L . A positive thermal gradient is introduced into the system along the z -axis by using $T_L = T_H - 0.1\epsilon/k_B$ or $T_L = T_H - 0.3\epsilon/k_B$.

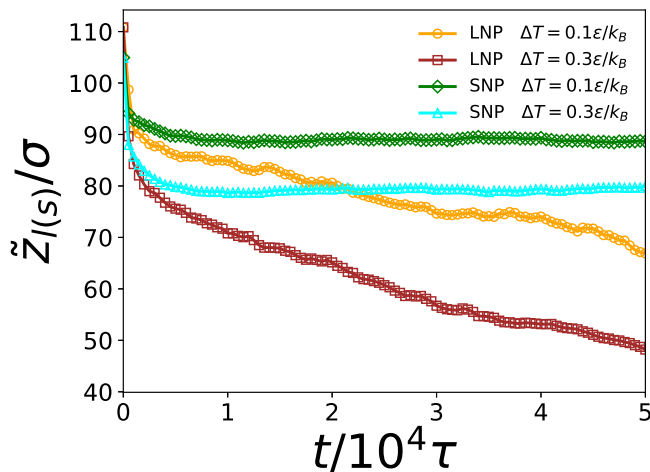


FIG. S3. Average positions of LNPs (orange circles and dark brown squares) and SNPs (green diamonds and cyan triangles) as a function of time after a positive thermal gradient along the z -axis is introduced into the system as described in Fig. S2. The data are for $\Delta T \equiv T_H - T_L = 0.3\epsilon/k_B$ (dark brown squares and cyan triangles) and $0.1\epsilon/k_B$ (orange circles and green diamonds).

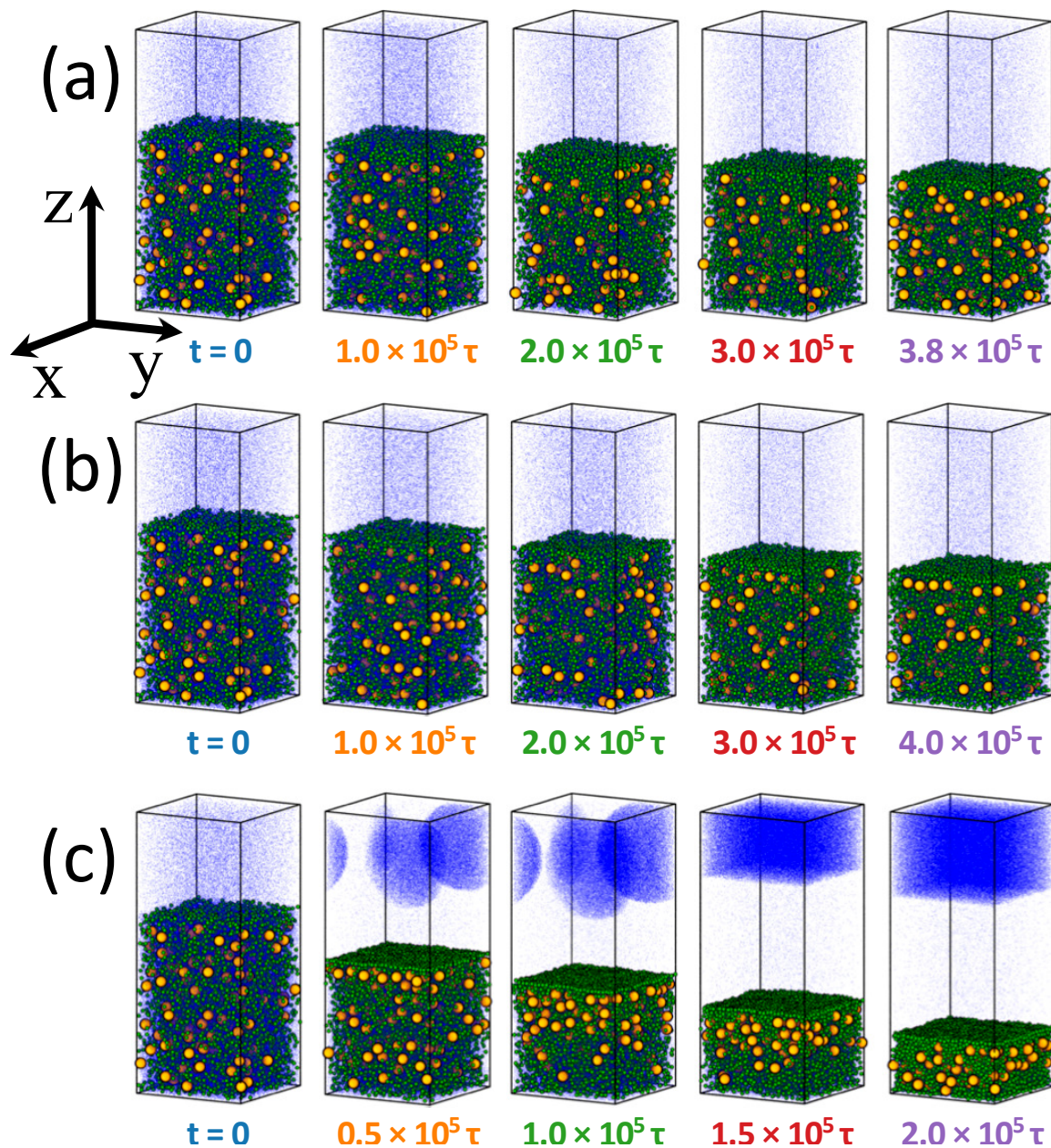


FIG. S4. Snapshots during solvent evaporation for (a) $T_{1.0}^l T_{1.1}^v \zeta_5$, (b) $T_{1.0}^l T_{1.05}^v \zeta_5$, and (c) $T_{1.0}^l T_{0.75}^v \zeta_5$. Elapsed time since evaporation was initiated at $t = 0$ is listed under each snapshot. Temperature and density profiles of the 5 systems are shown in Fig. S5. Color code: SNPs (green), LNPs (orange), and solvent (blue). Only 5% of the solvent beads are visualized to improve clarity.

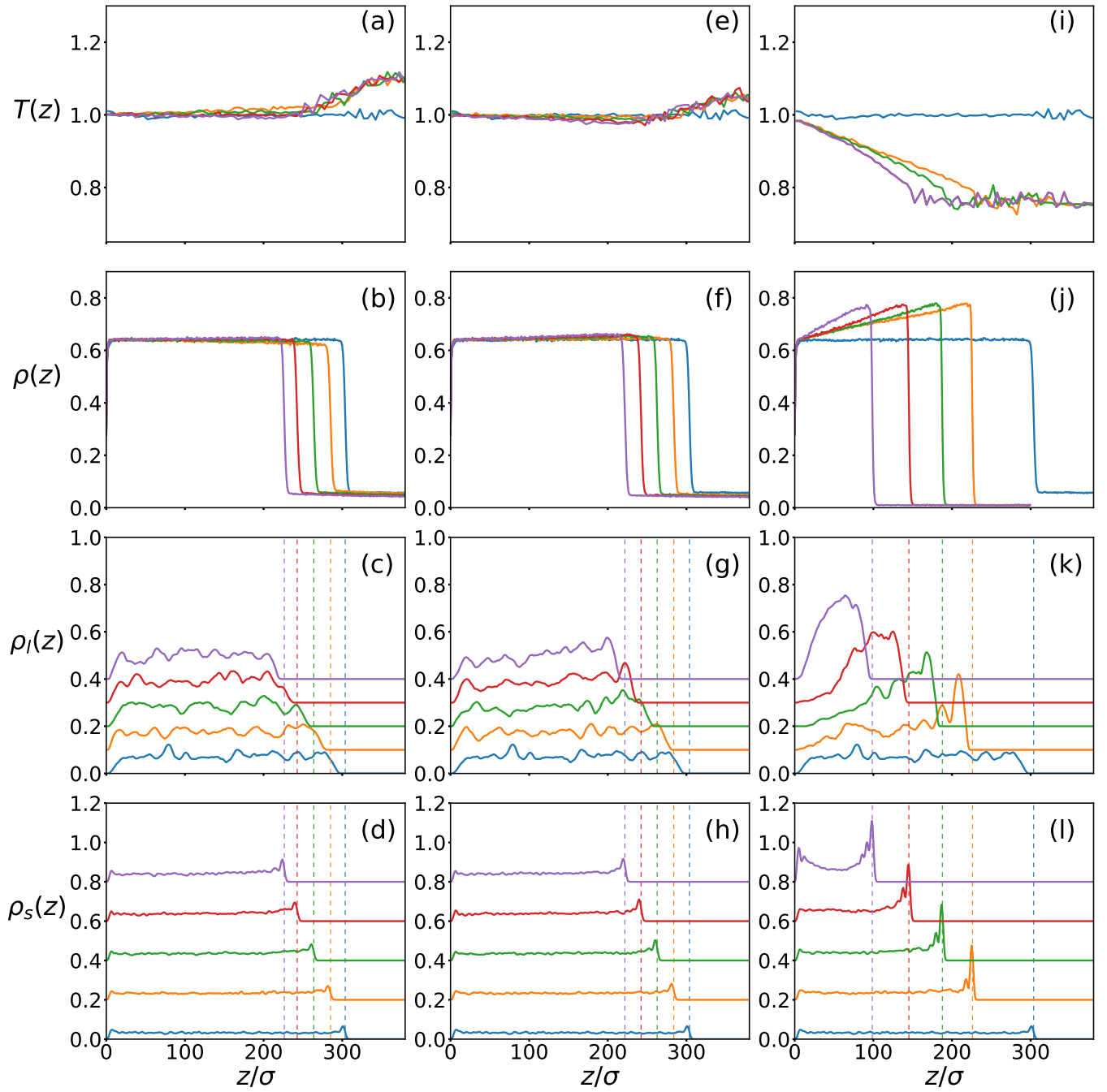


FIG. S5. Temperature profiles (top row) and density profiles for the solvent (second row), LNPs (third row), and SNPs (bottom row) for $T_{1.0}^l T_{1.1}^v \zeta_5$ (a-d), $T_{1.0}^l T_{1.05}^v \zeta_5$ (e-h), and $T_{1.0}^l T_{0.75}^v \zeta_5$ (i-l), respectively. The curves follow the same order as the snapshots shown in Fig. S4. The vertical dashed lines indicate the location of the liquid-vapor interface. For clarity, the density profiles for LNPs (SNPs) are shifted upward by $0.1m/\sigma^3$ ($0.2m/\sigma^3$) successively.

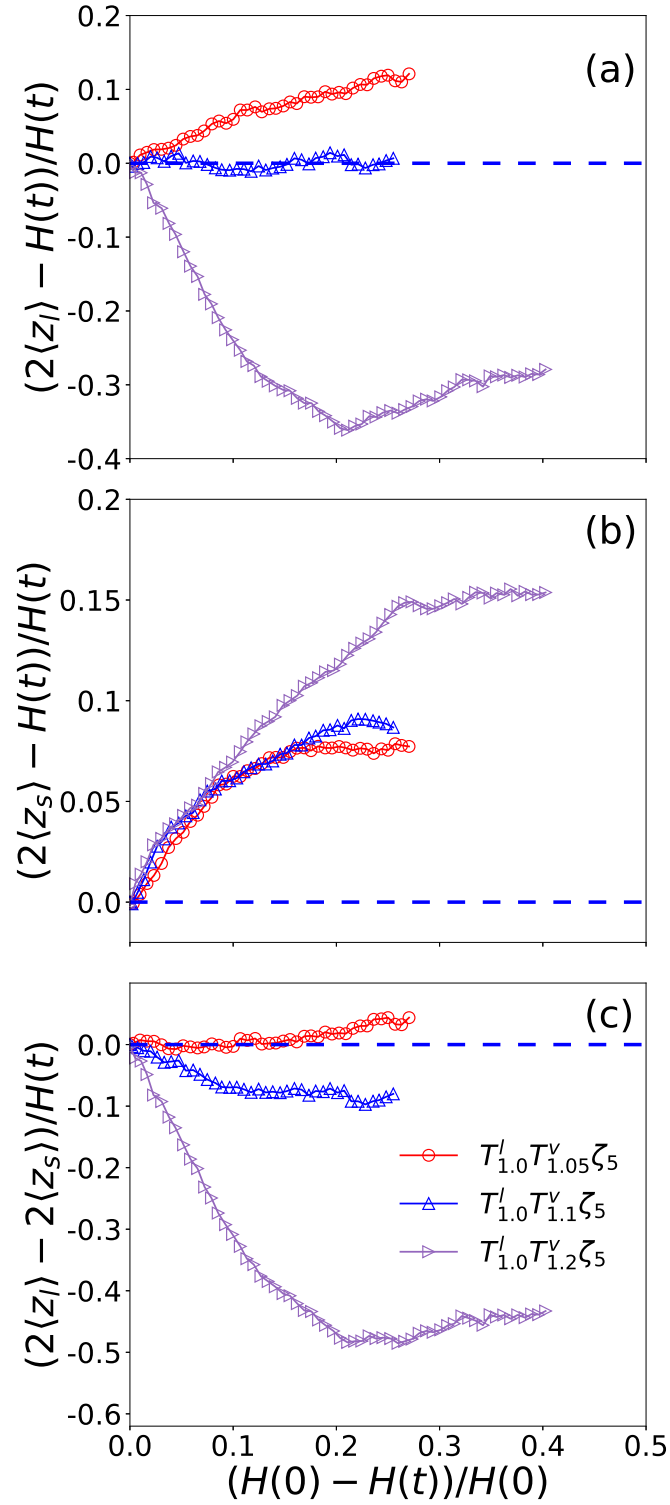


FIG. S6. Average position in the z direction relative to the center of the film, normalized by $H(t)/2$, is plotted against the extent of drying, quantified as $(H(0) - H(t))/H(0)$, for (a) LNPs and (b) SNPs. Panel (c) shows the average separation between LNPs and SNPs, normalized by $H(t)/2$, as a function of the extent of drying. Data are for $T_{1.0}^l T_{1.05}^v \zeta_5$ (red circles), $T_{1.0}^l T_{1.1}^v \zeta_5$ (blue triangles), and $T_{1.0}^l T_{1.2}^v \zeta_5$ (purple right-pointing triangles).

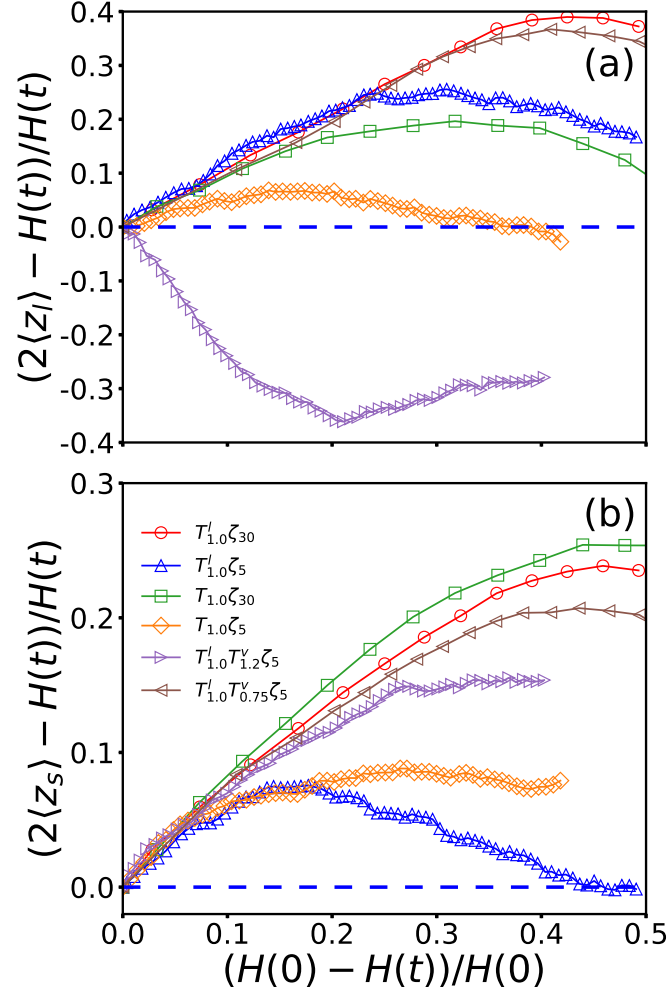


FIG. S7. Average position in the z direction relative to the center of the film, normalized by $H(t)/2$, is plotted against the extent of drying, quantified as $(H(0) - H(t))/H(0)$, for (a) LNPs and (b) SNPs. Data are for $T_{1.0}^l \zeta_{30}$ (red circles), $T_{1.0}^l \zeta_5$ (blue triangles), $T_{1.0} \zeta_{30}$ (green squares), $T_{1.0} \zeta_5$ (orange diamonds), $T_{1.0}^l T_{1.2}^v \zeta_5$ (purple right-pointing triangles), and $T_{1.0}^l T_{0.75}^v \zeta_5$ (brown left-pointing triangles).

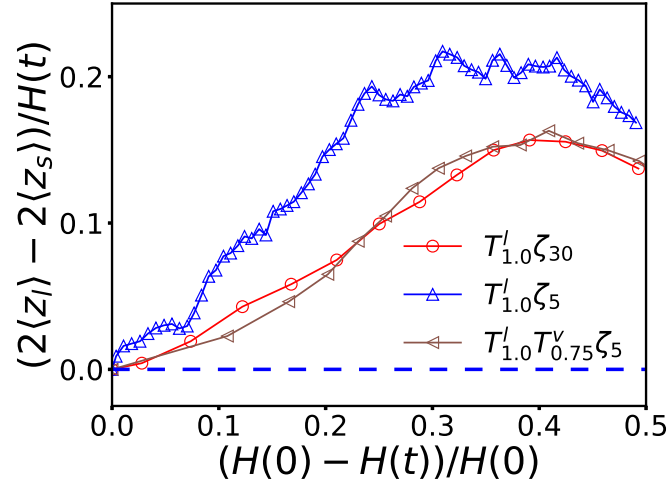


FIG. S8. Average position in the z direction relative to the center of the film, normalized by $H(t)/2$, is plotted against the extent of drying, quantified as $(H(0) - H(t))/H(0)$, for (a) LNPs and (b) SNPs. Panel (c) shows the average separation between LNPs and SNPs, normalized by $H(t)/2$, as a function of the extent of drying. Data are for $T_{1.0}^l \zeta_{30}$ (red circles), $T_{1.0}^l \zeta_5$ (blue triangles), and $T_{1.0}^l T_{0.75}^v \zeta_5$ (brown left-pointing triangles).

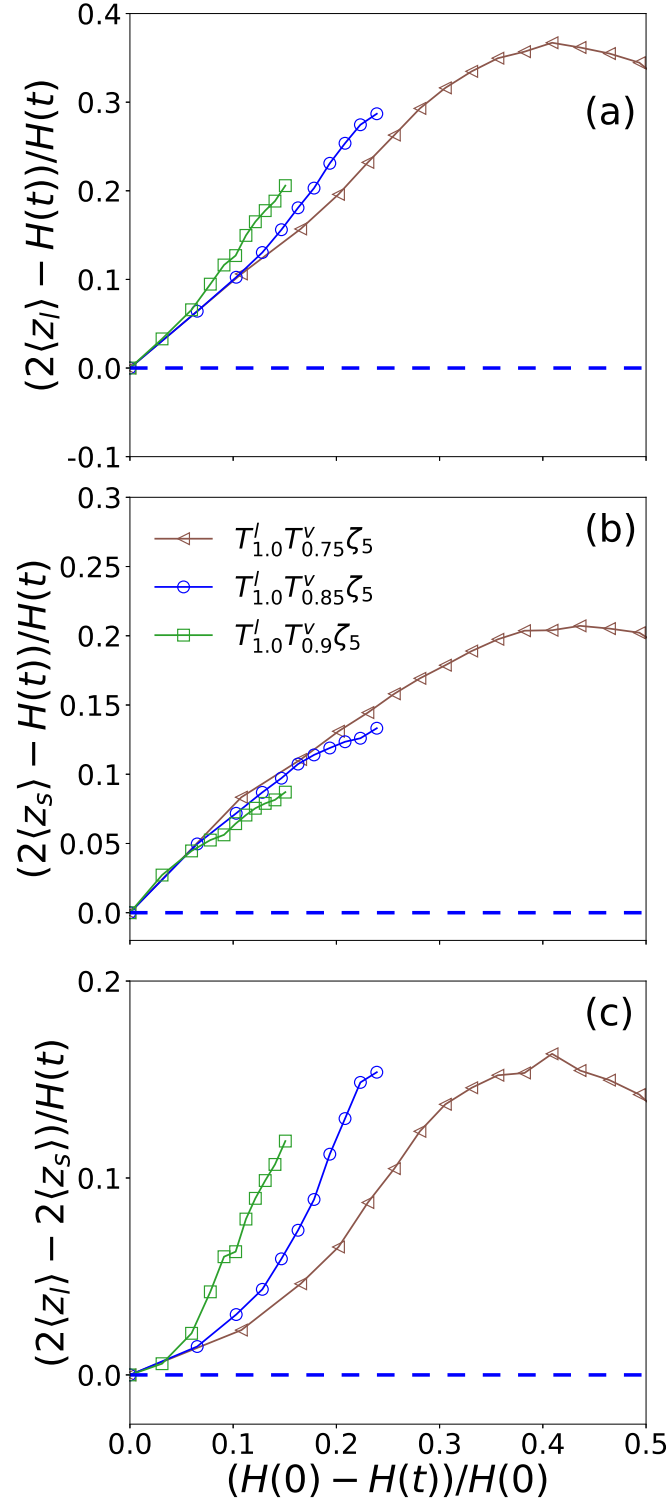


FIG. S9. Average position in the z direction relative to the center of the film, normalized by $H(t)/2$, is plotted against the extent of drying, quantified as $(H(0) - H(t))/H(0)$, for (a) LNPs and (b) SNPs. Panel (c) shows the average separation between LNPs and SNPs, normalized by $H(t)/2$, as a function of the extent of drying. Data are for $T_{1.0}^l T_{0.75}^v \zeta_5$ (brown left-pointing triangles), $T_{1.0}^l T_{0.85}^v \zeta_5$ (blue circles), and $T_{1.0}^l T_{0.9}^v \zeta_5$ (green squares).